# Two-dimensional and three-dimensional dynamic imaging of live biofilms in a microchannel by time-of-flight secondary ion mass spectrometry

Xin Hua,[1,2] Matthew J. Marshall,[3] Yijia Xiong,[4] Xiang Ma,[5] Yufan Zhou,[6] Abigail E. Tucker,[3] Zihua Zhu,[6] Songqin Liu,[1,a)] and Xiao-Ying Yu[2,a)]
[1]*School of Chemistry and Chemical Engineering, Southeast University, Nanjing, Jiangsu Province 211189, People's Republic of China*
[2]*Atmospheric Sciences and Global Climate Change Division, Pacific Northwest National Laboratory, Richland, Washington 99354, USA*
[3]*Biological Sciences Division, Pacific Northwest National Laboratory, Richland, Washington 99354, USA*
[4]*College of Osteopathic Medicine of the Pacific-Northwest, Western University of Health Sciences, Lebanon, Oregon 97355, USA*
[5]*Material Sciences, Pacific Northwest National Laboratory, Richland, Washington 99354, USA*
[6]*W. R. Wiley Environmental Molecular Science Laboratory, Pacific Northwest National Laboratory, Richland, Washington 99354, USA*

(Received 22 April 2015; accepted 24 April 2015; published online 5 May 2015)

A vacuum compatible microfluidic reactor, SALVI (System for Analysis at the Liquid Vacuum Interface), was employed for *in situ* chemical imaging of live biofilms using time-of-flight secondary ion mass spectrometry (ToF-SIMS). Depth profiling by sputtering materials in sequential layers resulted in live biofilm spatial chemical mapping. Two-dimensional (2D) images were reconstructed to report the first three-dimensional images of hydrated biofilm elucidating spatial and chemical heterogeneity. 2D image principal component analysis was conducted among biofilms at different locations in the microchannel. Our approach directly visualized spatial and chemical heterogeneity within the living biofilm by dynamic liquid ToF-SIMS. © *2015 AIP Publishing LLC*. [http://dx.doi.org/10.1063/1.4919807]

Mapping how metabolic pathways are interconnected and controlled at the subcellular scale within dynamic living systems continues to present a grand scientific challenge. Biofilms, consisting of aggregations of bacterial cells and extracellular polymeric substance (EPS), present an important avenue for deciphering complex microbial communities. During biofilm formation, cells assemble in a secreted polymer milieu of polysaccharides, proteins, glycolipids, and DNA.[1,2] Microfluidics provides unprecedented control over flow conditions, accessibility to real-time observation, high-throughput testing, and mimics *in vivo* biological environments.[3] An understanding of the mechanism underlying biofilm formation and the design of advanced microfluidic experiments could address challenges such as interpreting microbial community interactions, biofouling, and resistance to antimicrobial chemicals. However, only a handful of biofilm studies used microfluidic approaches that provided hydrated chemical imaging at high spatial resolution.[4–7] Most studies utilized confocal microscopy,[4] FTIR spectroscopy,[5] or other approaches (e.g., high density interdigitated capacitors[7]) for biofilm monitoring. Imaging mass spectrometry has been demonstrated in biofilm studies.[8,9] A coupled microfluidic-imaging mass spectrometry approach would provide the chemical molecular spatial mapping needed to better address the scientific challenge of biofilms.

Recently, we developed a portable microfluidic reactor, System for Analysis at the Liquid Vacuum Interface (SALVI),[10,11] which overcame the grand challenge of studying liquids with

a)Authors to whom correspondence should be addressed. Electronic addresses: liusq@seu.edu.cn and xiaoying.yu@pnnl.gov

 

high volatility and liquid interfaces using surface sensitive vacuum instruments. SALVI enables direct imaging of liquid surfaces using electron or ion/molecular based vacuum techniques. Our microfluidic approach used a polydimethylsiloxane (PDMS) microchannel fully enclosed with a thin silicon nitride (SiN) membrane (100 nm thick). For visualization, 2 $\mu$m diameter holes were opened in the SiN membrane *in vacuo*. These detection windows were dynamically drilled using the time-of-flight secondary ion mass spectrometry (ToF-SIMS) primary ion beam (e.g., $Bi^+$).[12]

Unlike liquid sample holders for transmission electron microscopy and scanning transmission electron microscopy, SALVI is self-contained and portable.[13] As a result, it can potentially be used in many finely focused analytical tool with minimal adaptation.[10] The analytical performance of SALVI has been demonstrated with a variety of analytes ranging from biology to material sciences.[14,15] Unlike most microfluidic applications that are only suitable under ambient conditions (e.g., separations, cell and small amount sample manipulation, and thermal flow-sensors),[16–18] SALVI is compatible with both *in situ* ambient and *in vacuo* spectroscopy analysis and imaging.[19] Biofilms have been successfully cultivated inside the microfluidic channel and imaged using correlative confocal laser scanning microscopy (CLSM) and ToF-SIMS.[20]

Our approach opens a new avenue to study biological sample in their natural state. Although ToF-SIMS has been widely used for providing molecular signatures of organic and biological molecules in complex biological systems[21,22] or lipid spatial mapping,[23] the vacuum-based ToF-SIMS generally requires solid (either dried[24] or cryo treated[25]) samples. Here, we report ToF-SIMS two dimensional (2D) and three dimensional (3D) chemical images of hydrated biofilms. *In situ* time and space-resolved identifications of fatty acid (FA) fragments characteristic of *Shewanella* are illustrated by 3D images reconstructed from the ToF-SIMS depth profile time series. Principal component analysis (PCA) further elucidates biofilm chemical and spatial heterogeneity and shows the key chemical component at different depth and location of the biofilm including the biofilm-surface attachment interface.

For all growth experiments, two samples were cultured simultaneously. At days 5 and 6, one sample was harvested for immediate analysis, respectively, using a ToF-SIMS V spectrometer (IONTOF GmbH, Münster, Germany). Similar results were obtained from both samples, because the biofilm-attachment surface was probed. For consistency, only day 6 data are shown here, while additional data are provided in the supplementary material.[28] 2D and 3D image visualizations were obtained using the IONTOF instrument software. PCA was performed using MATLAB R2012a (MathWorks, Inc., Natick, MA, USA). 2D images of .bif format were converted and integrated into a matrix. Data were pretreated by normalization to total ions, square root transformation, and then mean centering.[26] For m/z spectra PCA, unit mass peaks from m/z 199 to m/z 255 were used (see Figure S-2[28]). Unit mass peaks from m/z 1–300 were also used and results are comparable (see Figure S-3[28]). Five characteristic FA peaks (m/z 199, 213, 227, 241, and 255, corresponding to C12, C13, C14, C15, and C16 FAs) were used in image PCA.[27] Images representing each PC were reconstructed from the score matrix using the red, green, and blue (RGB) color scale.

Using depth profiling, we drilled through the SiN membrane and collected depth-resolved images of the live biofilm (Figure 1(a)). Our analysis of the negative ToF-SIMS spectra after SiN punch-through showed *Shewanella* FA fragments in the m/z 195–255 range.[20] From the depth profile time series, we selected five regions (highlighted as I, II, III IV, and V) within the FA m/z range to visualize 2D spatially resolved images collected for 46 s (1000 scans) before (I), during (II), or after (III, IV, V) SiN membrane punch-through.[20] When false color 2D images of FA fragments characteristic of *Shewanella* biofilms were selected from the dynamic depth profiling data, differences were observed (Figure 1(b)) among the five regions. Furthermore, the biofilm images after SiN membrane punch-through (III, IV, V) displayed variations across the 2 $\mu$m diameter surfaces, with C12 (m/z 199) being distributed across regions III, IV, and V and C15 (m/z 241) FAs mostly in region V (see Figure S-4 for additional FA images[28]). This suggested that depth-resolved chemical heterogeneities were present in the biofilm. To illustrate, we reconstructed the 2D images from depth profiling data within the biofilm region (from the beginning of III through the end of V) and show spatially resolved 3D

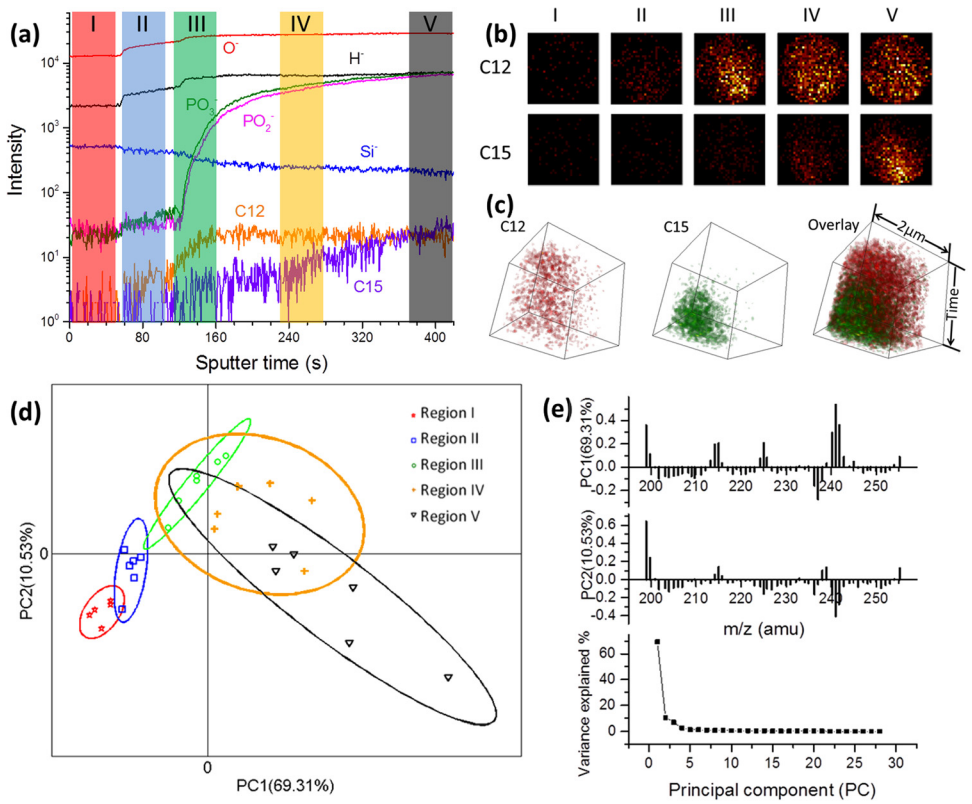


FIG. 1. (a) ToF-SIMS depth profiling of the day 6 biofilm attached to the SiN membrane in the microfluidic channel. Five regions representing sample before SiN punch-through (I) during punch-through (II) or within the biofilm region (III, IV, and V) are illustrated. (b) 2D false color images of day 6 biofilm FAs at the five time regions highlighted in (a). (c) Reconstructed 3D day 6 biofilm images showing FA fragment distributions within the entire biofilm region (III–V, 302 s). The time axis represents depth profiling from near the SiN surface into the biofilm. (d) Spectra PCA score plot of day 6 biofilm showing the differences and similarities among selected five regions (m/z 199–255). A 95% confidence limit for each region was defined by an ellipse with the same color to the corresponding region clusters. (e) Loadings of PC1 and PC2 corresponding to (d) and the plot of PC variance contributions.

chemical images within the entire sample (Figure 1(c) and movies S1-S3[28]). The reconstructed 3D images revealed the heterogeneous spatial distribution overlay for C12 (red) and C15 (green) FAs during 302 s biofilm depth profiling from day 5 (Figure S-5[28]) and day 6 (Figure 1(c)).

Spectral PCA was used to analyze the m/z spectra. The deepest region (V) into the biofilm was the most different from the other two biofilm regions (III and IV), further confirming the heterogeneities observed in the 2D images (e.g., C12 and C15 FA fragments) contributing most to this spatial difference. In addition, C12 FA fragments played a key role in the biofilms imaged near the SiN membrane attachment surface (III and IV). When inspected individually, C12 FAs were observed throughout the entire biofilm region, suggesting that C12 FA fragments may play a role in biofilm attachment to a surface and they may be main components of EPS throughout the biofilm. In contrast, C15 FAs were more abundant deeper within the biofilm, indicating that they may be more relevant to bacteria cells themselves.

Uniform sputtering rate was assumed during depth profiling. To better determine the depth and shape of the SIMS ionization crater, AFM measurements were collected using an agarose sample in the SALVI reactor as a proxy for the biofilms (Figure S-6[28]). The AFM results showed that the 100 nm SiN was drilled through and confirmed that the biofilm interface was probed by ToF-SIMS. Ideally, real-time correlative AFM and ToF-SIMS measurements will be needed due to the self-healing property of biofilms. However, such capability is currently under development.

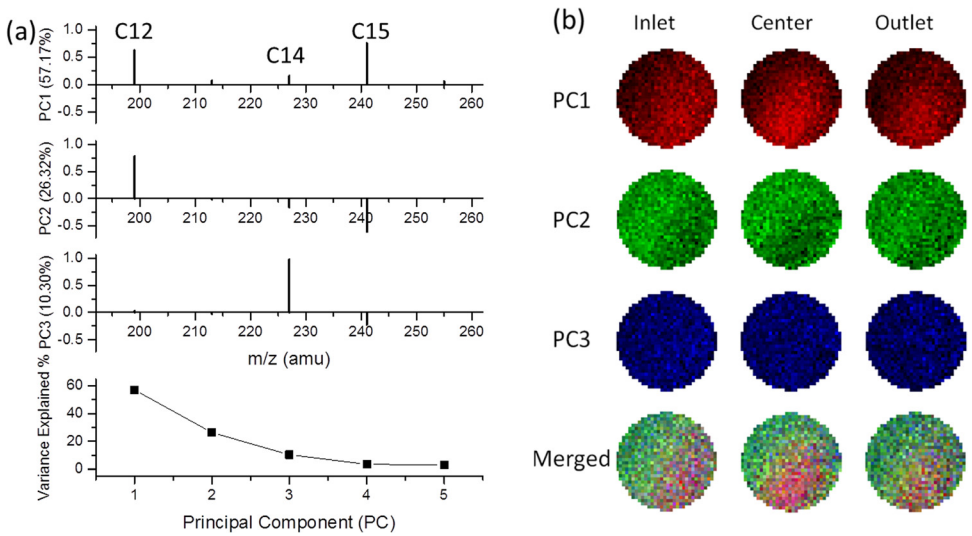


FIG. 2. (a) Image PCA loading plots illustrating the contribution of each FA peak in the day 6 biofilm at three locations within the microfluidic channel. The variance contributions of each PC are shown at the bottom. (b) Reconstructed false-color 2D PCA images in RGB corresponding to each PC scores at these locations along the microfluidic channel. The RGB composite images of the three key PCs are depicted in the bottom. Only data within the 2 $\mu$m diameter circle were considered in analysis.

To further analyze chemical differences within biofilms, we performed ToF-SIMS depth profiling at three locations along the microchannel; namely, the inlet, center, and outlet as illustrated in Figure S-1(b).[28] At each location, we defined the five regions described in Figure 1(a), and 2D image PCA analysis was conducted on the biofilm region (from the beginning of III through the end of V) to visualize the chemical distributions on day 6. Figure 2(a) shows the loading plots for the m/z peaks that contribute to each PC image (Figure 2(b)). The first three PCs explained 93.79% of the variance within the data. For PC1, the strongest positive loading fragments were C12 and C15 FAs, which are the bright red areas in three PC1 images. The C12 FAs were the main contributor to the green regions in the PC2 image. The strongest loading for PC3 in blue was C14 FAs. Compared to PC1 and PC2, PC3 played a limited contribution to the overall spatial distribution discrimination. The merged images give a demonstration of chemical spatial distribution of key components of biofilms in the liquid microenvironment.

Our results show that SALVI and liquid ToF-SIMS studies of live biofilms offer dynamic, depth-resolved chemical mapping and produce 2D and 3D visualizations of spatial heterogeneity within a biofilm. Chemical imaging of biofilms near the attachment interface can enhance our understanding of biofilm formation in environmental, medical, and industrial settings. Our approach provides a universal portable platform and enables *in situ* probing of complex living biological systems potentially across multiple time and space scales. Because of the portability and vacuum compatibility, SALVI offers a valuable linkage with proteomic mass spectrometry via microfluidics and a non-destructive package for integrative *in situ* analysis of live biological systems in system biology.

We are grateful for the support from the Chemical Imaging Initiative-Laboratory Directed Research and Development and the Quick Deployment Funds of the Pacific Northwest National Laboratory (PNNL). Biofilm studies were also funded by a U.S. DOE Office of Science Early Career Research Award (60385, M.J.M.). The authors thank Dr. Daniel Graham for his suggestions on PCA analysis, Dr. Bingwen Liu and Dr. Li Yang for their assistance in SALVI fabrication, Mr. William Chrisler for CLSM imaging, Ms. Zhaoying Wang for ToF-SIMS operation, and Ms. Zhuoran Duan for MATLAB programming. The research was performed in the W. R. Wiley Environmental Molecular Sciences Laboratory, a National Scientific User Facility sponsored by the DOE and located at PNNL. PNNL is operated for DOE by Battelle. A U.S. patent (20140038224 A1) was filed by Battelle.

[1]H. C. Flemming and J. Wingender, Nat. Rev. Microbiol. **8**(9), 623–633 (2010).
[2]G. Lambert, A. Bergman, Q. Zhang, D. Bortz, and R. Austin, New J. Phys. **16**(4), 045005 (2014).
[3]J. Kim, M. Hegde, S. H. Kim, T. K. Wood, and A. Jayaraman, Lab Chip **12**(6), 1157–1163 (2012).
[4]Y. Yawata, K. Toda, E. Setoyama, J. Fukuda, H. Suzuki, H. Uchiyama, and N. Nomura, J. Biosci. Bioeng. **110**(3), 377–380 (2010).
[5]H.-Y. N. Holman, R. Miles, Z. Hao, E. Wozei, L. M. Anderson, and H. Yang, Anal. Chem. **81**(20), 8564–8570 (2009).
[6]T. Ahmed and R. Stocker, Biophys. J. **95**(9), 4481–4493 (2008).
[7]L. Richter, C. Stepper, A. Mak, A. Reinthaler, R. Heer, M. Kast, H. Bruckl, and P. Ertl, Lab Chip **7**(12), 1723–1731 (2007).
[8]C. Bhardwaj, Y. Cui, T. Hofstetter, S. Y. Liu, H. C. Bernstein, R. P. Carlson, M. Ahmed, and L. Hanley, Analyst **138**(22), 6844–6851 (2013).
[9]G. L. Gasper, L. K. Takahashi, J. Zhou, M. Ahmed, J. F. Moore, and L. Hanley, Anal. Chem. **82**(17), 7472–7478 (2010).
[10]L. Yang, X. Y. Yu, Z. H. Zhu, T. Thevuthasan, and J. P. Cowin, J. Vac. Sci. Technol. A **29**(6), 061101 (2011).
[11]L. Yang, X. Y. Yu, Z. H. Zhu, M. J. Iedema, and J. P. Cowin, Lab Chip **11**(15), 2481–2484 (2011).
[12]X.-Y. Yu, L. Yang, J. Cowin, M. Iedema, and Z. Zhu, U.S. patent 8,555,710 (15 October 2013).
[13]X. Y. Yu, B. W. Liu, and L. Yang, Microfluid Nanofluid **15**(6), 725–744 (2013).
[14]L. Yang, Z. H. Zhu, X. Y. Yu, E. Rodek, L. Saraf, T. Thevuthasan, and J. P. Cowin, Surf. Interface Anal. **46**(4), 224–228 (2014).
[15]L. Yang, Z. Zhu, X.-Y. Yu, S. Thevuthasan, and J. P. Cowin, Anal. Methods **5**(10), 2515–2522 (2013).
[16]B. G. Chung, J. W. Park, J. S. Hu, C. Huang, E. S. Monuki, and N. L. Jeon, BMC Biotechnol. **7**(60), 60 (2007).
[17]Y. C. Wang and P. Dimitrakopoulos, Phys. Fluids **18**(8), 082106 (2006).
[18]L. Guerin, M. Bossel, M. Demierre, S. Calmes, and P. Renaud, Transducers **1**, 1419–1422 (1997).
[19]B. Liu, X.-Y. Yu, Z. Zhu, X. Hua, L. Yang, and Z. Wang, Lab Chip **14**(5), 855–859 (2014).
[20]X. Hua, X.-Y. Yu, Z. Wang, L. Yang, L. Bingwen, Z. Zhu, A. E. Tucker, W. B. Chrisler, E. A. Hill, T. Thevuthasan, Y. Lin, S. Liu, and M. J. Marshall, Analyst **139**(7), 1609–1613 (2014).
[21]E. J. Lanni, S. S. Rubakhin, and J. V. Sweedler, J. Proteomics **75**(16), 5036–5051 (2012).
[22]M. K. Passarelli, A. G. Ewing, and N. Winograd, Anal. Chem. **85**(4), 2231–2238 (2013).
[23]M. L. Kraft and H. A. Klitzing, Biochim. Biophys. Acta **1841**(8), 1108–1119 (2014).
[24]J. F. C. de Brouwer, K. E. Cooksey, B. Wigglesworth-Cooksey, M. J. Staal, L. J. Stal, and R. Avci, J. Microbiol. Methods **65**(3), 562–572 (2006).
[25]S. G. Ostrowski, C. T. Van Bell, N. Winograd, and A. G. Ewing, Science **305**(5680), 71–73 (2004).
[26]D. J. Graham and D. G. Castner, Biointerphases **7**(1–4), 49 (2012).
[27]D. J. Graham and D. G. Castner, Mass Spectrom. **2**(special-issue), S0014 (2013).
[28]See supplementary material at http://dx.doi.org/10.1063/1.4919807 for additional experimental descriptions and figures.